LEIDEN UNIVERSITY

Study of BCG-Substracted Images of Nearby Clusters

by

Juan Manuel Espejo Salcedo

Advisor:

Dr. Henk Hoekstra

Natural Sciences Faculty
Sterrenwacht

April 2017

"Not only is the Universe stranger than we think, it is stranger than we can think.."

Werner Heisenberg

Abstract

Natural Sciences Faculty
Sterrenwacht

(This is just a simple draft taken from the original idea) We have obtained deep imaging data for a sample of low redshift massive clusters. The light from the BGC overwhelms the images from background galaxies and faint cluster members in the cluster core, and needs to be carefully subtracted. This is expected to reveal background galaxies that are strongly lensed. Identifying such systems allows for unique follow-up studies. Also the number density of faint cluster members may tell us something about the dynamical state of the cluster and how BGCs form. The aim of this project is to model the BCG light and search for strong lensing candidates and study the properties of faint cluster members in the core..

Acknowledgements

I would like to thank ...

Contents

List of Figures

List of Tables

Dedicated to my parents, whose love and support are my biggest motivation...

Chapter 1

Introduction

Stellar mass to light ratio and Stellar populations in the BCGs

Galaxy Clusters

IMF is a very fundamental and important quantity in the study of stellar systems because it constraints the physics of star formation but also because it allows us to infer stellar masses through observed luminosities.

the correct use of an IMF in the context of gravitational lensing on massive objects like early type galaxies in galaxy clusters can help us constraint the amount of stellar mass and thus also infer the amount of dark matter in these systems.

Studying the amount of dark matter contribution, one could in principle make a good estimation of the stellar mass-to-light ratio.

Mass-to-light ratios of early-type galaxies are of particular interest to understand the tilt of the fundamental plane. Virial relations imply that the effective surface brightness $I_{\rm eff}$, the effective radius $r_{\rm eff}$ and the central velocity dispersion σ_0 in hot stellar systems are not independent of each other. This is revealed by the fundamental plane of early type galaxies.

The Salpeter IMF implies more low-mass stars and a higher mass-to-light ratio. In the R-band the scaling between the two cases is $\Upsilon_{\rm Salp} \approx 1.56\Upsilon_{\rm Krou}$

For galaxies that are far away, it is impossible to make star counts, for this reason, the mass to light ratio of the stellar population provides a simple constraint on the IMF (Russell J. Smith and John R. Lucey)

Strong gravitational lensing of background galaxies provides a useful method to determine masses in elliptical galaxies, since it is difficult to constraint the IMF via M/L

massive galaxies - Salpeter is a good IMF

A Koupra IMF finds a value of Υ of around 4 for the mass to light ratio. (R. J. Smith 2014)

DM fraction in comparison with the IMF

Studying the matter distribution given by strong gravitational lensing can give us information about the iMF of the BCGs

percentage of dark matter will allow me to define the IMF more precisely. I want to see what fraction of the mass, what fraction of the surface density is stars.

At very small radii stars dominate the lensing mass, so that lensing provides a direct probe of the stellar mass-to-light ratio, with only small corrections needed for dark matter (Russell Smith and John R. Lucey 2013)

Salpeter is heavier than Kroupa

Salpeter mass function is $n(M) \propto M^{-2.3}$

For spiral galaxies, the most used IMFs are Chabrier or Kroupa, but for elliptical galaxies, constraining the IMF via $M_\star/L$ poses a greater challenge since masses are more difficult to establish for dynamically-hot systems. This is where gravitational lensing plays an important role.

As said before, bulges appear to have heavier IMFs than disks (Dutton et. al 2013)

"Large M/L ratios could arise either from an excess of faint dwarf stars in a "bottom heavy" IMF, or from an excess of dark remnants in a "top heavy" IMF" (Russell J. Smith and John R. Lucey 2013).

Modelling the lensing configuration provides the total projection mass within an aperture.

strong lensing at different radii is useful.

if I got to certain radius I will have more dark matter, because light drops quickly.

basically find how much dark matter and hoy many stars are there in the profile

Two interesting questions about the BCGs:

1. Where are they located

2. What is their stellar populations

Chapter 2

Theoretical Framework

Tyter.

2.1 Galaxy Clusters

Glas.

dwarf stars contribute very little to the integrated light from an old stellar population (Smith 2015)

Galaxy clusters contain a population of stars gravitationally unbound to individual galaxies, yet still bound to the clusters overall gravitational potential, created by the stripping of stars from galaxies during interactions and mergers

FIGURE 2.1: Galaxy Cluster MACS 1206, credits to NASA Hubble Space Telescope

Quoted (need to change this):The image of galaxy cluster MACS J1206.2-0847 (or MACS 1206) is part of a broad survey with NASA Hubble Space Telescope.The distorted shapes in the cluster are distant galaxies from which the light is bent by the gravitational pull of an invisible material called dark matter within the cluster of galaxies. This cluster is an early target in a survey that will allow astronomers to construct the most detailed dark matter maps of more galaxy clusters than ever before.These maps are being used to test previous, but surprising, results that suggest that dark matter is more densely packed inside clusters than some models predict. This might mean that galaxy cluster assembly began earlier than commonly thought.

Scientists are planning to observe a total of 25 galaxy clusters under a project called CLASH (Cluster Lensing and Supernova survey with Hubble).One of the first objects observed for the new census is the galaxy cluster MACS J1206.2-0847. This conglomeration of galaxies is one of the most massive structures in the universe, and its gigantic gravitational pull causes stunning gravitational lensing. MACS 1206 lies 4 billion light-years from Earth. In addition to curving of light, gravitational lensing often produces double images of the same galaxy. In the new observation of cluster MACS J1206.2-0847, astronomers counted 47 multiple images of 12 newly identified galaxies.The era when the first clusters formed is not precisely known, but is estimated to be at least 9

billion years ago and possibly as far back as 12 billion years ago. If most of the clusters in the CLASH survey are found to have excessively high accumulations of dark matter in their central cores, then it may yield new clues to the early stages in the origin of structure in the universe.

2.2 Gravitational Lensing

Galaxies and clusters of galaxies that act as gravitational lenses can be approximated by single isothermal spheres. It is easy to relate an angular scaling parameter ξ_E, referred to as the Einstein radius, to the mass inside the corresponding light cone. The Einstein radius corresponds to the ring image of a point source aligned exactly on the axis of the lens.

Summary of isothermal sphere:

$$\rho(r) = \frac{\sigma^2}{2\pi G r^2} \tag{2.1}$$

$$\Sigma(\xi) = \frac{\sigma^2}{2G\xi} \tag{2.2}$$

$$\xi_E = 4\pi \left(\frac{\sigma}{c}\right)^2 \frac{D_{ds}}{D_s} \tag{2.3}$$

In reality, the density profile and lensing properties of galaxies is a bit more complicated than the assumption of a singular isothermal sphere, so we need to take into account more complex but elaborate profiles as the NFW (Navarro, Frenk, White, 1996).

The NFW density profile is

$$\rho(r) = \frac{\delta_c \rho_c}{(r/r_s)(1 + r/r_s)^2} \tag{2.4}$$

where the characteristic overdensity (dimensionless quantity) is given by:

$$\delta_c = \frac{200}{3} \frac{c^3}{\ln(1+c) - c/(1+c)} \tag{2.5}$$

The concentration parameter c is strongly correlated with Hubble type, c=2.6 separating early from late-type galaxies. Those galaxies with concentration indices $c > 2.6$ are

early-type galaxies reflecting the fact that the light is more concentrated towards their centres, its formal definition in terms of the virial and characteristic radius is:

$c = r_{200}/r_s$

Dutton and Maccio 2014 (in continuation of previous studies such as Munoz Cuartas et. al.), made simulations of halo masses from dwarf galaxies to galaxy clusters and find constraints on the concentration parameter for different redshifts, the relation between the concentration parameter with redshift and virial mass is shown in the following figure:

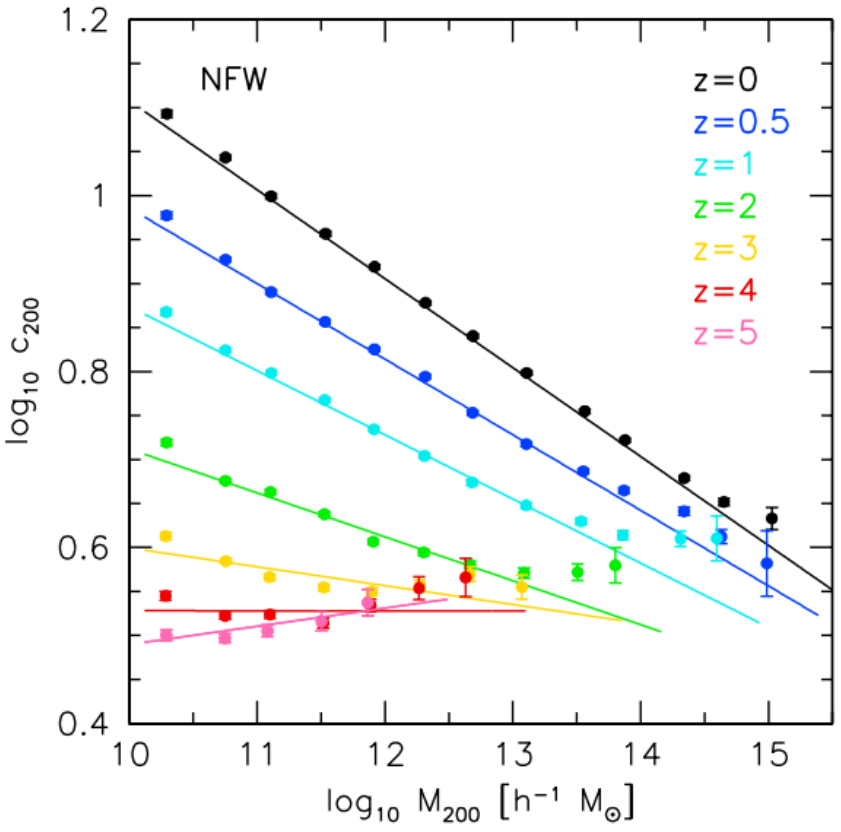

FIGURE 2.2: Evolution of the concentration mass relation, by Dutton & Maccio, 2014

let's take the case of ABELL1068, it's magnitude in U is 21.94, in I is 18.46, in g is 20.09, in r is 19.5, also $M_{200} = 4.3 \times 10^{14} M_\odot$ (van der Burg et. al 2015)

The bolometric luminosity of Abell1068 is 10^{44}erg/s that in solar luminosities is $1.9 \times 10^{12} L_\odot$, this gives an effective brightness of $0.962 \times 10^7 M_\odot/kpc^2$.

the distance to the galaxy is 591.42857 Mpc

In the case of the ABELL1068 cluster, our estimation yields a concentration parameter of 4.46.

The surface mass density in the NFW profile is given by:

$$\Sigma_{\mathrm{NFW}}(x) = \begin{cases} \frac{2r_s\delta_c\rho_c}{(x^2-1)}\left[1 - \frac{2}{\sqrt{1-x^2}}\operatorname{arctanh}\sqrt{\frac{1-x}{1+x}}\right](x<1) & (x<1) \\ \frac{2r_s\delta_c\rho_c}{3}(x=1) & (x=1) \\ \frac{2r_s\delta_c\rho_c}{(x^2-1)}\left[1 - \frac{2}{\sqrt{x^2-1}}\arctan\sqrt{\frac{x-1}{1+x}}\right](x<1) & (x>1) \end{cases} \tag{2.6}$$

then the concentration parameter for ABELL1068 is about 7.9 supposing a mass of the galaxy of $10^{12.5}M_{\odot}$

so from the critical density:

$$\rho_c = \frac{3H^2(z)}{8\pi G} \tag{2.7}$$

The critical density would be: 2×10^{-26} in SI units so in $M_{\odot}/pc^3$ it is 2.9×10^{-7}

$H(z) = H_0(1 + \Omega z)^{3/2}$

the Hubble parameter at z=0.138 is H(z)=85.6

The characteristic radius is given by $r_{1/2} = 1.34R_e$

For the stellar content of the cluster we can use de Vaucouleurs law for the surface brightness distribution in giant elliptical galaxies which is:

$$I(R) = I_e e^{-b\left[(R/R_e)^{1/4}-1\right]} \tag{2.8}$$

where $b = 7.67$ and I_e is the effective brightness which is basically the brightness at the effective radius R_e

From the paper of Lokas and Mamon, for constant mass-light-ratio we have $\Sigma_M(R) = \Upsilon I(R)$ where $I(R) \approx 10^7$ was found by fitting the surface brightness with *GALFIT*.

The mass to light ratio is $\Upsilon \approx 4$

Hence we have the surface mass density for both the stellar content and the NFW profile:

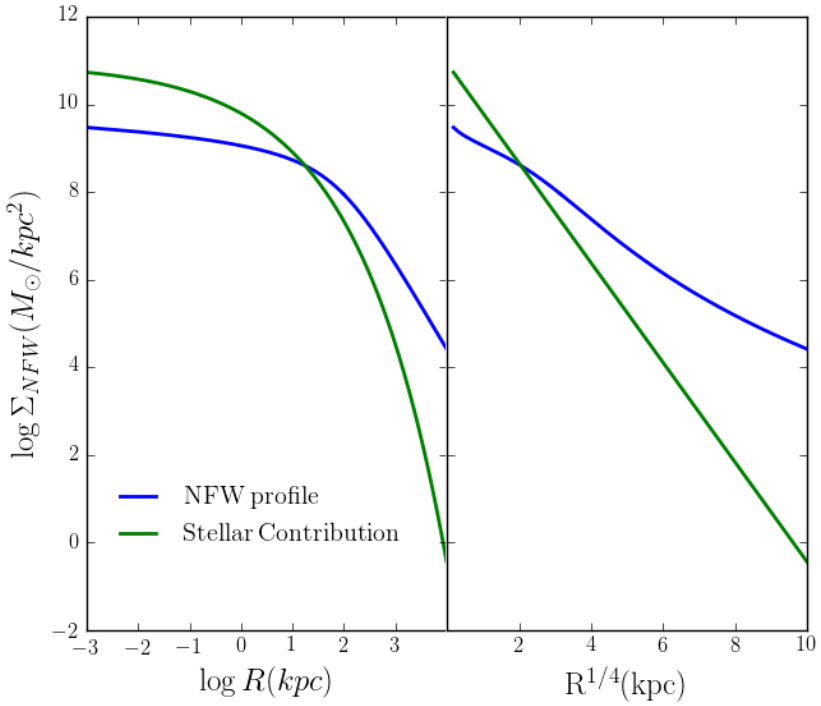

FIGURE 2.3: Surface mass density profiles in logarithmic and $R^{1/4}$ scale for the NFW profile and the stellar component.

But we are more interested in the enclosed mass which can be done by integrating the surface mass density:

$$M(R) = \int_0^R 2\pi R\Sigma(R)dR \tag{2.9}$$

And we can recover our luminosity by integrating the surface brightness profile accordingly:

$$L = \int_0^R 2\pi RI(R)dR \tag{2.10}$$

The integration gives a value that is comparable to the one found using Faber-Jackson relation: $L = \Upsilon \times \sigma^4 \approx 1.2 \times 10^{12} M_\odot$

The plot for the enclosed mass is:

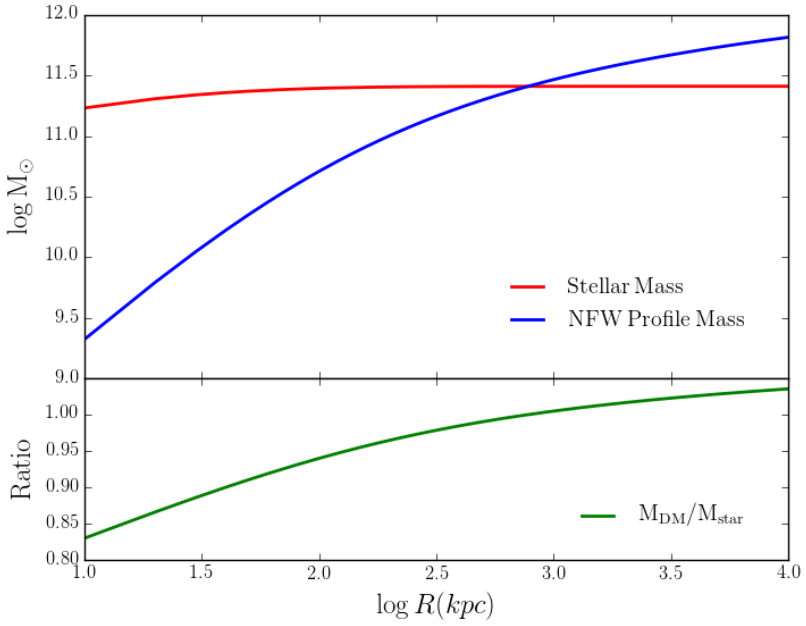

FIGURE 2.4: Enclosed mass and DM to stellar mass ratio

The value found for the mass in light is $M_\star = 2.582 \times 10^{11} M_\odot$ and the mass given by the NFW profile is $M_{\rm NFW} = 6.557 \times 10^{11} M_\odot$.

Now, we are interested in having an accurate estimate of the Einstein radius to constraint the model, so we make different analysis on the radial dependence on the lensing properties such as shear, reduced shear and magnification.

The radial dependence on the shear is:

$$\gamma_{\rm NFW}(x) = \begin{cases} \frac{r_s \delta_c \rho_c}{\Sigma_c} g_<(x) & (x < 1) \\ \frac{r_s \delta_c \rho_c}{\Sigma_c} \left[\frac{10}{3} + 4 \ln\left(\frac{1}{2}\right)\right] & (x = 1) \\ \frac{r_s \delta_c \rho_c}{\Sigma_c} g_>(x) & (x > 1) \end{cases} \tag{2.11}$$

where:

$$g_<(x) = \frac{8 \operatorname{arctanh} \sqrt{\frac{1-x}{1+x}}}{x^2 \sqrt{1-x^2}} + \frac{4}{x^2} \ln\left(\frac{x}{2}\right) - \frac{2}{(x^2-1)} + \frac{4 \operatorname{arctanh} \sqrt{\frac{1-x}{1+x}}}{(x^2-1)\,(1-x^2)^{1/2}} \tag{2.12}$$

$$g_<(x) = \frac{8 \arctan \sqrt{\frac{x-1}{1+x}}}{x^2 \sqrt{x^2-1}} + \frac{4}{x^2} \ln\left(\frac{x}{2}\right) - \frac{2}{(x^2-1)} + \frac{4 \arctan \sqrt{\frac{x-1}{1+x}}}{(x^2-1)^{3/2}} \tag{2.13}$$

and with the critical surface mass density:

$$\Sigma_c \equiv \frac{c^2}{4\pi G}\frac{D_s}{D_d D_{ds}} \tag{2.14}$$

these equations come from the paper Wright and Brainerd 1999

the plot of the shear dependence on the radius is:

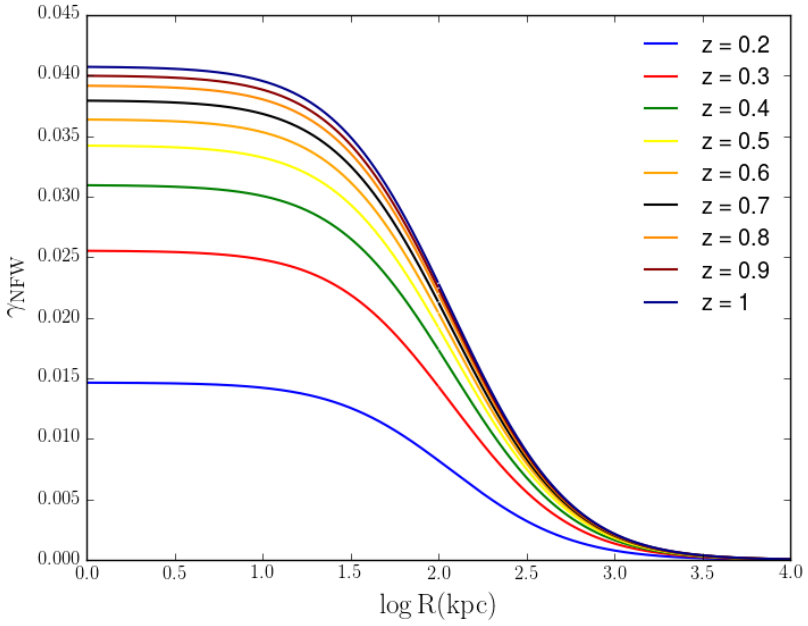

FIGURE 2.5: Shear dependence on radius for different redshift of the background galaxies

The magnification tensor is:

$$\frac{\partial\beta}{\partial\theta} = \delta_{ij} - \frac{\partial^2\psi}{\partial\theta_i\partial\theta_j} = \begin{pmatrix} 1-\kappa-\gamma_1 & -\gamma_2 \\ -\gamma_2 & 1-\kappa+\gamma_1 \end{pmatrix} \tag{2.15}$$

The total magnification μ is given by the determinant of the magnification tensor:

$$\mu = \frac{1}{(1-\kappa)^2 - \gamma_1^2 - \gamma_2^2} \tag{2.16}$$

Where κ is the convergence that determines the magnification and γ_1 and γ_2 are the shear components that determine the distortion of the background objects.

The magnification is then:

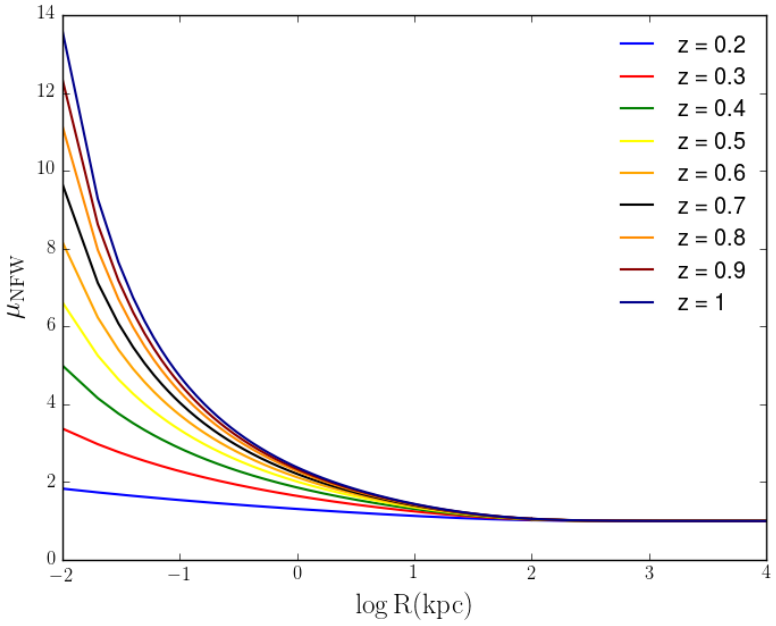

FIGURE 2.6: Magnification radial profile for various redshifts

The reduced shear is given by:

$$g = \frac{\gamma}{1 - \kappa} \tag{2.17}$$

The reduced shear for background objects at different redshifts is:

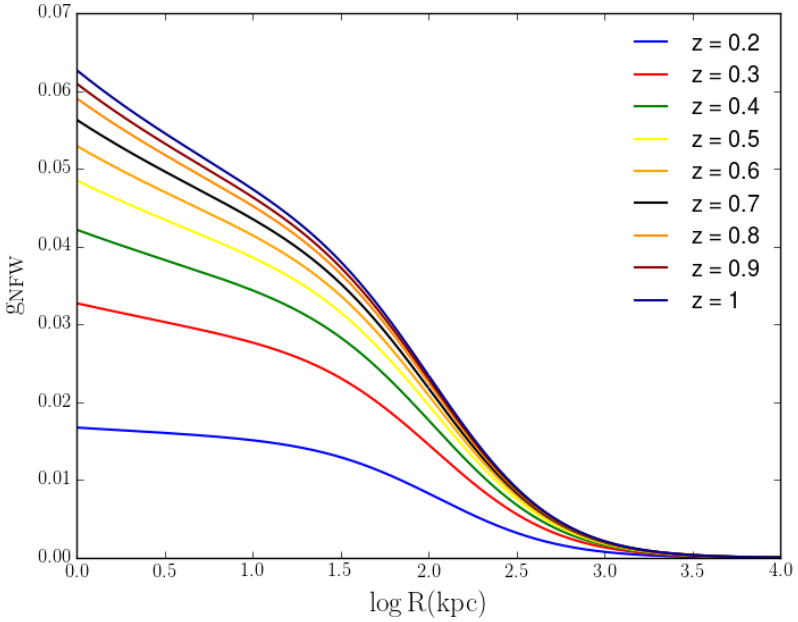

FIGURE 2.7: Reduced shear radial profile for different redshifts.

so we get the Einstein ring where μ is infinite or when g is 1 (k=1/2)

2.3 IMF in BCGs

number of stars per unit mass

Kroupa, Chabrier, Salpeter,

Heavyweight

It's difficult to see how much of the faint stars contribute to the mass of the system. We only see the new bright ones

BCG -¿ giant ellipticals

For stars, measurements of the luminosity function can be used to derive the Initial Mass Function (IMF). For galaxies, this is more difficult because Mass to light ratio (M/L) of the stellar population depends upon the star formation history of the galaxy.

bulges have heavier IMFs than disks

Several recent studies have presented evidence for "heavyweight" IMFs in giant ellipticals, with a mass-to-light-ratio twice that of a Milky Way like IMF.

Chapter 3

Observational Procedures

the full description of the survey is in: D. J. Sand et. al. 2011

MegaCam wide field imager on the CFHT (Canada-France-Hawii Telescope). The cluster sample consisted of 101 clusters within the range of redshifts from 0.05 ¡ z¡ 0.55

58 clusters from the MENEACs (Multi-Epoch nearby cluster survey)

The meneacs clusters represent all clusters in the BAX X-ray cluster database that are observable for the CFHT

About 60 clusters, but we used only 30 for the final studies and paid special attention to 10, marked with *

G, U, I and R images

The original images have dimensions of [11000:11000] pixels but since our relevant region is the center of the cluster where the BCG is located, we cut the images with dimension of [1000,1000] for the color analysis and [4000:4000] to characterize the colors and discriminate between cluster and non-cluster members.

The INT images were multiple exposures so it was necessary to make a mosaic of them using SWARP.

3.1 Sextractor

Segmentation image that will be used as a mask image (bad pixels) for GALFIT

We need to discriminate between field stars and the galaxies of the cluster so in order to do this, we used some of the parameters found by *SEXTRACTOR* that allow us to

Cluster	z	$\sigma(km/s)$	$d(Mpc)$	$\theta_E(")$
A1033	0.126	762	540	14.6155
A1068*	0.138	740	591.4	13.5945
A1132	0.136	727	582.9	13.1515
A119*	0.044	875	188.6	21.0798
A1413*	0.143	881	612.9	19.1569
A1650	0.084	720	360	13.6758
A1651	0.085	903	364.3	21.4876
A1795	0.062	778	265.7	16.3514
A2029*	0.077	1152	330	35.2776
A2050	0.118	854	505.7	18.5258
A2055	0.102	697	437.1	12.5642
A2064	0.108	675	462.9	11.7048
A2065*	0.073	1095	312.9	32.0110
A2069	0.116	966	497.1	23.7574
A2142*	0.091	1086	390	30.8756
A2319*	0.056	1101	240	32.9563
A2420	0.085	800	364.3	16.8653
A2440	0.091	766	390	15.3608
A2597	0.085	682	364.3	12.2569
A2627	0.126	800	540	16.1096
A2703	0.114	800	488.6	16.3307
A399	0.072	800	308.6	17.1049
A553	0.066	800	282.9	17.2155
A655*	0.127	800	544.3	16.0911
A754*	0.054	800	231.4	17.4367
A763	0.085	800	364.3	16.8653
A795	0.136	800	582.9	15.9252
A85*	0.055	800	235.7	17.4182
A961	0.124	800	531.4	16.1464
A990	0.144	800	617.1	15.7778

TABLE 3.1: Abell clusters and their redshifts as given by C. Bildfell et. al. 2012. Marked with * the chosen clusters with the most promising features

constraint the fitted data. These are class-star, flux_radius, and FWHM (full wicth half maximum). Class-star uses the neural network star/galaxy of *SEXTRACTOR* that will give values close to 1 for stars and 0 for galaxies. flux_radius, and FWHM are closely related to each other and give the radius which contains half of the light of the object so it will be small for stars and bigger for extended objects.

In order to extract the same objects and make the segmentation masks for the desired objects in the different filters, we used SEXTRACTOR on dual mode

Color magnitude diagram for A1068

we used a zero point magnitude of 30

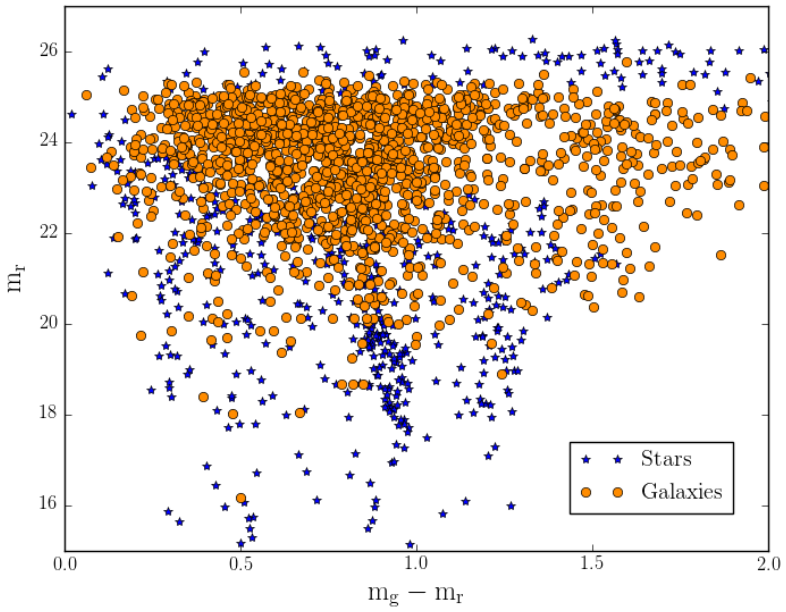

FIGURE 3.1: Color Magnitude diagram of A1068 with the differentiation of stars from galaxies

Mag vs flux rad to discriminate

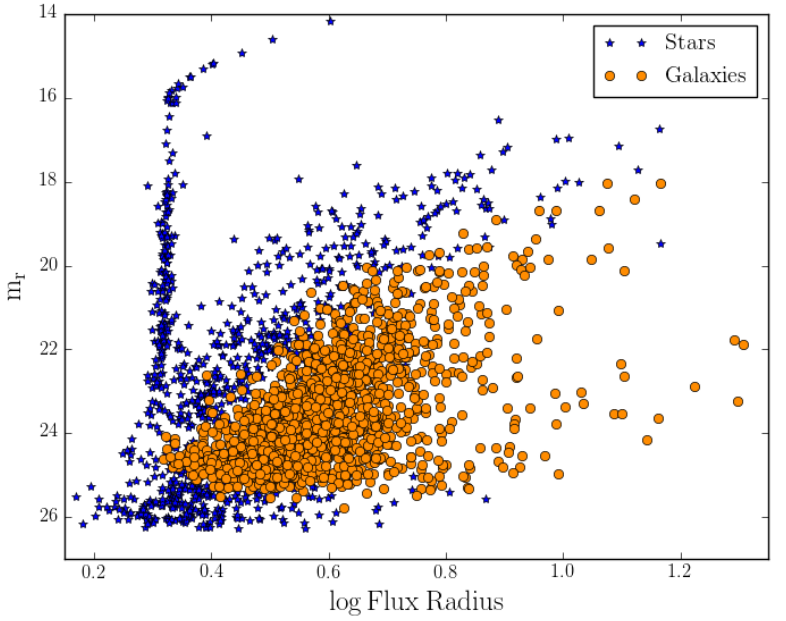

FIGURE 3.2: Magnitude vs Flux radius of A1068 to identify the galaxies using the criteria of their flux distribution

3.2 Galfit

GALFIT (Peng et. al) fits two dimensional profiles so it is a useful tool to remove the light from the BCG and allow us to observe background objects

Fit Sersic profiles with n=4 which is de Vaucouleurs profile.

A first run gives us a rough idea of the true position of the center of the BCG so we can set this values in a second run for each cluster. We needed to combine different Sersic parameters, as well as Fourier and bending modes for some of the BCGs.

We use the segmentation masks given by *SEXTRACTOR* to mask bright objects in the fitting of the BCG

the fitting of many objects (not only the BCG)

the best results were given when we masked the innermost region of the BCG so the fitting will put more weight in the rest of the profile, thus reducing most of the light that hides the background objects.

we have to take into account the magnification bias

The parameters C0, B1, B2, F1, F2, etc. listed below are hidden from the user unless he/she explicitly requests them. These can be tagged on to the end of any previous components except, of course, the PSF and the sky – although *GALFIT* won't bar you from doing so, and will just ignore them. Note that a Fourier or Bending mode amplitude of exactly 0 will cause *GALFIT* to crash because the derivative image *GALFIT* computes internally will be entirely 0. If a Fourier or Bending amplitude is set to 0 initially *GALFIT* will reset it to a value of 0.01. To prevent *GALFIT* from doing so, one can set it to any other value.

Bending modes B1) 0.07 1 Bending mode 1 (shear) B2) 0.01 1 Bending mode 2 (banana shape) B3) 0.03 1 Bending mode 3 (S-shape)

Azimuthal fourier modes F1) 0.07 30.1 1 1 Az. Fourier mode 1, amplitude and phase angle F2) 0.01 10.5 1 1 Az. Fourier mode 2, amplitude and phase angle F6) 0.03 10.5 1 1 Az. Fourier mode 6, amplitude and phase angle F10) 0.08 20.5 1 1 Az. Fourier mode 10, amplitude and phase angle F20) 0.01 23.5 1 1 Az. Fourier mode 20, amplitude and phase angle

Traditional Diskyness/Boxyness parameter c C0) 0.1 0 traditional diskyness(-)/boxyness(+)

The masks:

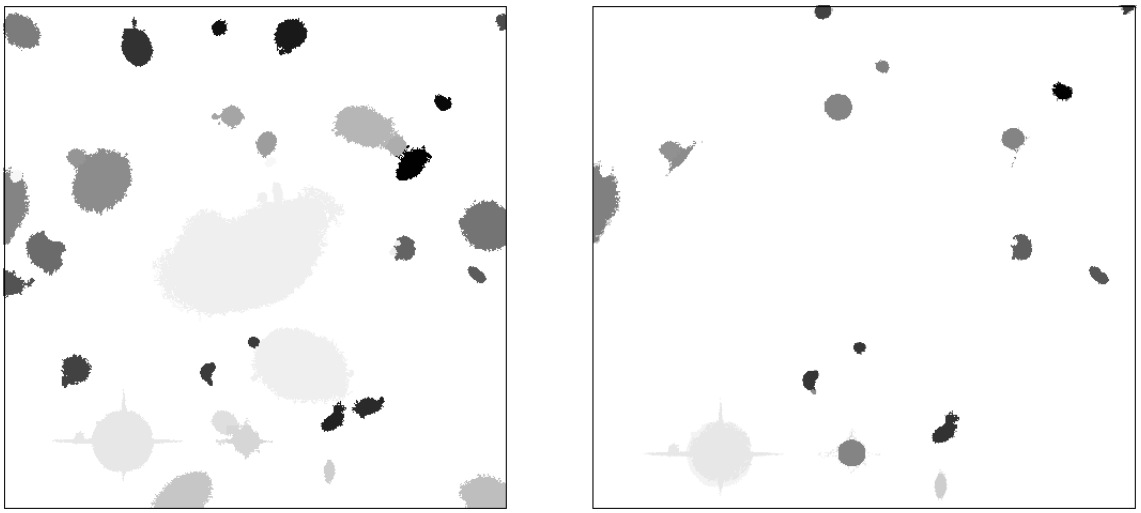

FIGURE 3.3: Segmentation images produced by SEXTRACTOR and used as mask files for the galfit extraction. Left panel is the original mask with all the bright objects. Right panel is the mask after the substraction of the regions surrounding the cluster galaxies to be fitted with GALFIT.

The colors are inverted for an easier visualization of the image. The fainter regions are actually the most luminous objects because *GALFIT* assigns increasing numbers starting from the brightest one, that is the BCG in this case

The original image, the fitted models and the output are presented here:

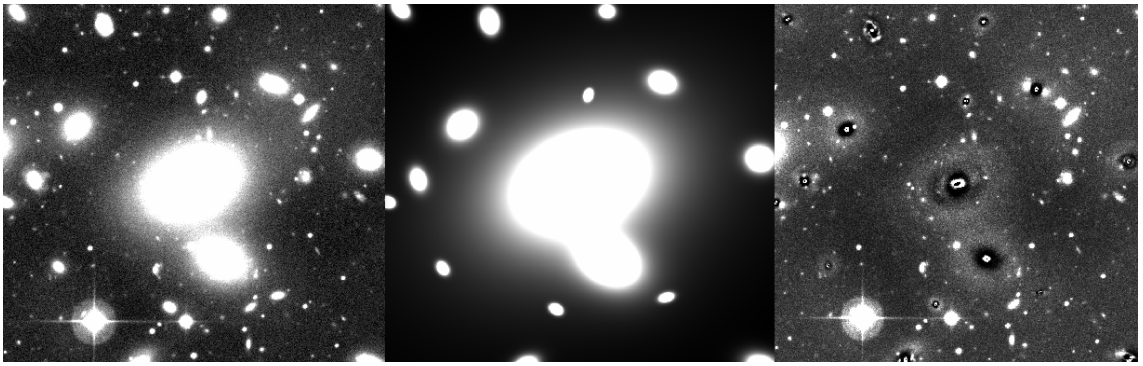

FIGURE 3.4: Galfit procedures. Left: Original image in zscale with the clear BCG expanding across a significant region of the central area. Middle:The models fitted by GALFIT for all the selected cluster galaxies. Right:Residual image after the substraction of the model galaxies.

3.3 Color images

We use IRAF to make the color images using our g,r,u,i bands

Here we take an isothermal sphere to model the Einstein ring in a distance of background objects of z=1

We made a color image of the original center of the cluster without subtracting the BCG in order to differentiate between cluster members from background galaxies and field stars. This allows us to fit only the cluster galaxies.

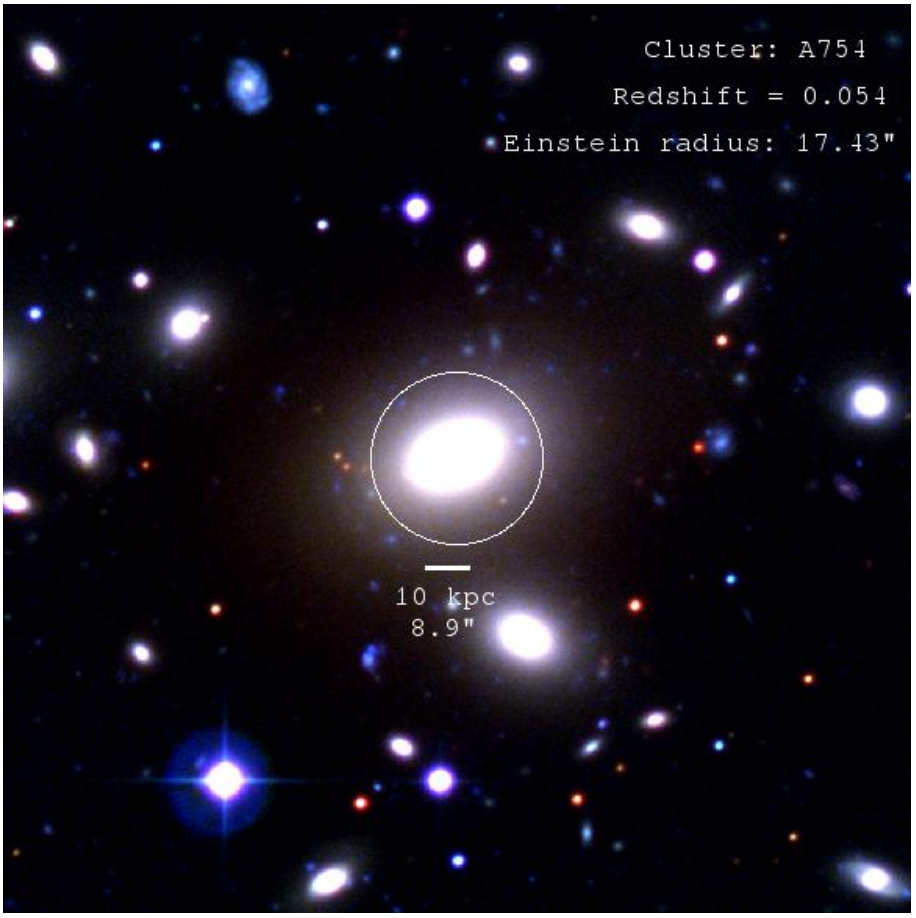

FIGURE 3.5: Color image of A754 cluster (filters i,g,u) with its Einstein radius calculated for an isothermal sphere of a background object at $z = 1$.

After choosing the galaxies that belong to the cluster by comparing their relative colors, we subtracted them using *GALFIT* and made the color image again changing the scaling values with the task CONVERT of IRAF so that we see can see the color contrast to search for good candidates of lensed objects. By looking at this reduced color image, we have another visual constraint to choose the clusters in which it would be worth to do photometric redshifts and search for objects with the same redshift in different locations around the very center of the BCG (object that has suffered strong lensing).

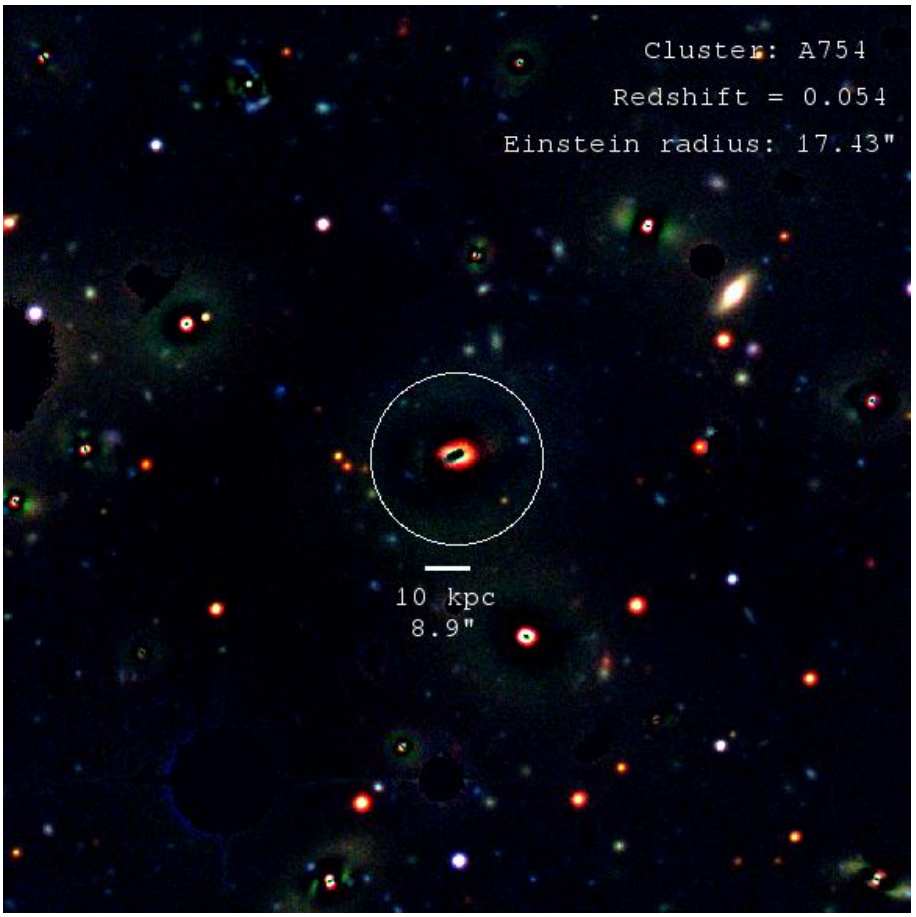

FIGURE 3.6: Color image of A754 cluster (filters i,g,u) after the substraction of the bright cluster galaxies.

Because we have 4 bands we were able to make different color images to see the contrast and make combinations that would allow us to see better the very red and very blue objects, in the following figure we have the g-r, i-r-g and i-g-u color images for three clusters.

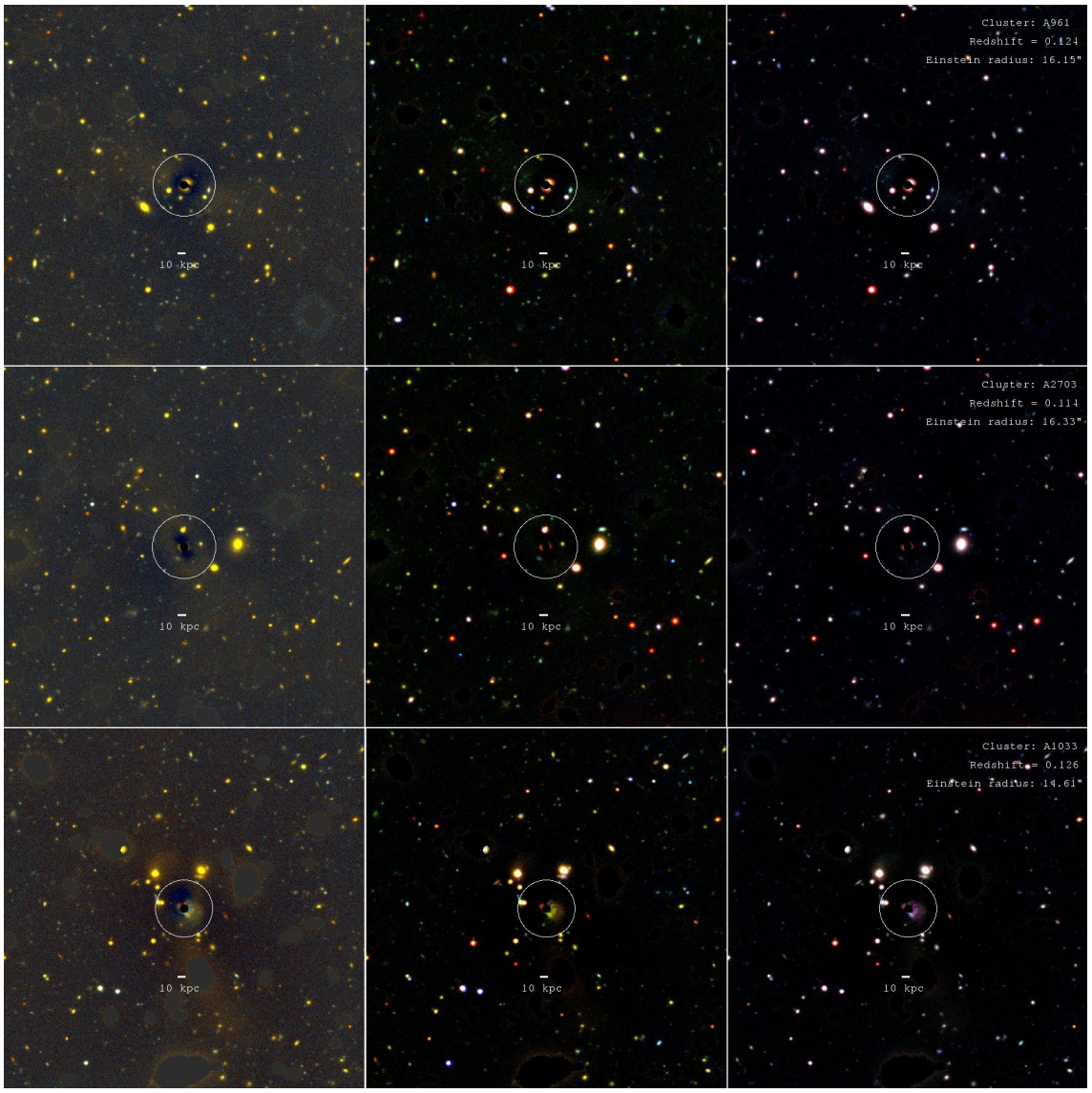

FIGURE 3.7: Different color images for different combination of the g,r,u,i filters for the clusters A961, A2703, A1033. Left column for the images constructed only with the g and r filter, central column for i,g,r and right column for i,g,u.

3.4 Photometric Redshift

We use the *COSMOS2015* (Laigle et. al 2016.) catalogue that contains photometric redshift of over half million galaxies in multiple bands to put another constraint in our study.

We use the matched catalogue for CFHT by —– and use the r-band. Our limiting magnitude is 23 in that band so we estimate the number of galaxies per redshift bin that we would expect to see in our sample with that limiting magnitude.

This sets an interesting constraint on what to expect in the inner region of the BCG and give us more information about where to search for good candidates.

The limiting magnitude is found using *SEXTRACTOR* that gives a good confidence on the detection of objects.

(using as reference Benitez, Narciso 2000)

To measure the photometric redshift of the galaxies (after filtering out the stars) in the inner region of the cluster after the subtraction of the BCG, we use the photometric redshift code EAZY (Brammer et. al 2008) which uses an extensive collection of spectral energy distributions for galaxies in the range $0 < z < 4$. Fortunately, the code includes library from CFHT in the I and U bands but doesn't have the filters in the G and R bands so I used the SUBARU survey filter information to be able to compute the photometric redshifts using four bands.

If you find this code useful, please include a citation to "Brammer, van Dokkum and Coppi, 2008, ApJ, 686, 1503" in the bibliography of any published work that makes use of EAZY.

Chapter 4

Study of images

We ter.

Chapter 5

Conclusions

Thes.

Bibliography

[1] Treu, Tommaso. 2010 *Strong Lensing by Galaxies*. Annu. Rev. Astron. Astrophysics. 2010. 48:87-125.

[2] R. F. J. Van der Burg et. al. 2015 *Evidence for the inside-out growth of the stellar mass distribution in galaxy clusters since z1̃*. preprint arXiv:1412.2137v2.

[3] Binney J., Tremaine S. *Galactic Dynamics*. Princeton University Press, 1994.

[4] C. O. Wright & Teresa G. Brainerd, Teresa. 1999 *Gravitational Lensing by NFW halos*. preprint arXiv:astro-ph/9908213v1.

[5] Smith, Russell. 2014 *Variations in the initial mass function in early-type galaxies: a critical comparison between dynamical and spectroscopic results*. MNRASL 443, L69-L73 (2014).

[6] C. Bildfell et. al. 2012 *Evolution of the red sequence giant to dwarf ratio in galaxy clusters out to z0̃.5*. MNRAS 425, 204-221 (2012).

[7] Smith, Russell & Lucey, John. 2013 *A giant elliptical galaxy with a lightweight initial mass function*. MNRAS 000, 1-14 (2013).

[8] R. J. Smith et. al. 2015 *The IMF-sensitive 1.14-μm Na I doublet in early-type galaxies*. MNRAS 000, 1-14 (2013).

[9] C. Sifon et. al. 2015 *Constraints on the alignment of galaxies in galaxy clusters from 1̃4000 spectroscopic members*. A&A 575, A48 (2015).

[10] S. M. Adams et. al. 2012 *The environmental dependence of the incidence of galactic tidal features*. The Astrophysical Journal, 144:128(11pp) (2012).

[11] D. J. Sand et. al. 2011 *Intracluster supernovae in the multi-epoch nearby cluster survey*. The Astrophysical Journal, 729:142 (13pp) (2011).

[12] J. C. Muñoz Cuartas et. al. 2010 *The redshift evolution of ΛCDM halo parameters: concentration, spin and shape*. MNRAS, 000,1-11 (2010).